Supplementary Information

Destruction of cell topography, morphology, membrane, inhibition of respiration, biofilm formation and bioactive molecule production by nanoparticles of Ag, ZnO, CuO, TiO_2 and Al_2O_3 towards beneficial soil bacteria

Bilal Ahmed,*[1] Fuad Ameen[2], Asfa Rizvi[1], Khursheed Ali[1], Hana Sonbol[3], Almas Zaidi[1], Mohammad Saghir Khan[1], Javed Musarrat[1,4]

[1]Department of Agricultural Microbiology, Aligarh Muslim University, Aligarh 202002, India

[2]Department of Botany and Microbiology, College of Science, King Saud University, Riyadh 11451, Saudi Arabia

[3]Department of Biology, College of Science, Princess Nourah bint Abdulrahman University, Riyadh, Saudi Arabia

[4]School of Biosciences and Biotechnology, Baba Ghulam Shah Badshah University, Rajouri, Jammu & Kashmir, India

***Correspondence to:**

Bilal Ahmed

Nanotoxicology Laboratory,

Department of Agricultural Microbiology,

Aligarh Muslim University, Aligarh 202002, India

Email; bilalahmed.amu@gmail.com

Table S1: FTIR bond assignments of *P. mosselii* in the presence and absence of Ag-NPs and ZnO-NPs

S. No.	IR signal (cm^{-1}) in the spectrum of *P. mosselii*			Frequency assignment	Reference
	Control	***P. mosselii* + AgNPs**	***P. mosselii* + ZnONPs**		
1	3324-3437	3319-3437	3333-3442	O–H str of hydroxyl groups	Maquelin et al. (2002)
2	3289	3292	3289	N–H str (amide A) of proteins	Maquelin et al. (2002)
3	3075	3072	3079	N–H str (amide A) of proteins	Maquelin et al. (2002)
4	2959	2959	2961	C–H str (asym) of $–CH_3$ in fatty acids	Maquelin et al. (2002)
5	2924	2926	2926	C–H str (asym) of $>CH_2$	Maquelin et al. (2002)
6	2853	2853	2853	CH_2 Sym lipids	Movasaghi et al. 2008
7	1650	1653	1653	Amide I of beta-pleated sheet structures	Maquelin et al. (2002)
8	1539	1540	1536	N-H def., C-H str	Movasaghi et al. (2008)
9	1442	1445	1445	Asy CH_3 bending of proteins	Movasaghi et al. (2008)
10	1400	1403	1405	Symmetric stretch of C-O of COO- groups	Lu et al. (2011)
11	1308	1314	1311	Amide III band components of proteins	Movasaghi et al. (2008)
12	1235	1235	1235	P=O str (asym) of $>PO_2$ phosphodiesters	Maquelin et al. (2002)
13	1066	1058	1072	P=O str (sym) of $>PO_2$	Maquelin et al. (2002)
14	600-900	600-900	600-900	Finger Print Region	Maquelin et al. (2002)

Table S2: FTIR bond assignments of *A. chroococcum* in the presence and absence of Ag-NPs and ZnO-NPs

S. No.	IR signal (cm^{-1}) in the spectrum of *A. chroococcum*			Frequency assignment	Reference
	Control	***A. chroococcum* + AgNPs**	***A. chroococcum* + ZnONPs**		
1	3324-3439	3319-3435	3314-3425	O–H str of hydroxyl groups	Maquelin et al. (2002)
2	3282	3284	3285	N–H str (Amide A) of proteins	Maquelin et al. (2002)
3	2956	2961	2961	C–H str (asym) of $–CH_3$ in fatty acids	Maquelin et al. (2002)
4	2924	2924	2924	C–H str (asym) of $>CH_2$	Maquelin et al. (2002)
5	2853	2850	2855	CH_2 Sym lipids	Movasaghi et al. (2008)
6	1653	1656	1653	Amide I of beta-pleated sheet structures	Maquelin et al. (2002)
7	1542	1539	1539	N-H def., C-H str	Movasaghi et al. (2008)
8	1457	1454	1451	Asy CH_3 bending of proteins	Movasaghi et al. (2008)
9	1402	1402	1396	Symmetric stretch of C-O of COO- groups	Lu et al. (2011)
10	1231	1235	1235	P=O str (asym) of $>PO_2$ phosphodiesters	Maquelin et al. (2002)
11	1072	1055	1058	P=O str (sym) of $>PO_2$	Maquelin et al. (2002)
12	600-900	600-900	600-900	Finger Print Region	Maquelin et al. (2002)

Table S3: Physicochemical properties of nanoparticles

Particulars	Nanoparticles				
	Al_2O_3-NPs	**CuO-NPs**	**TiO_2-NPs**	**ZnO-NPs**	**Ag-NPs**
[a]Elemental composition (%)	Al (50.6), O (49.4)	Cu (76.7), O (23.3)	Ti (53.2), O (46.8)	Zn (78.9), O (21.1)	Ag (38.01), C (2.47), N (18.88), O (33.93), Na (6.71)
[b]Morphology	Spherical to lobular to short rods of variable length and diameter	Irregular individual and aggregates with rough surface	Spherical with uniform size distribution	Pleomorphic, smaller to larger sized aggregates with some small thin sheets	Aggregates of NPs with various shapes predominantly spherical,
[c]Crystal size (nm)	28	18	4.6	24	12
[d]Primary size (nm)	21.8±8.7	18.4±5.5	3.9±0.9	34±10	13.2±9.5
[e]Secondary size (nm) in distilled water	238±4.6	194±5.8	148±8.4	248±11.7	221±12.4
Zeta potential (mV)	+26.1±1.7	-29.8±2.1	+19.2±2.3	-21±0.9	+31±3.1
Signal in FTIR spectrum (cm^{-1})	466	533	541	482	Various signals for quercetin functional groups such as -OH phenolic stretch, C-C stretches, C-H bending, C=O stretch and C-O stretch

[a]Data measured by EDX; [b]revealed by SEM, AFM and TEM; [c]measured by XRD; [d]Determined by TEM; [e]Determined by DLS. In this and succeeding tables, EDX, SEM, AFM, TEM, XRD and DLS represents energy dispersive X-ray, scanning electron microscopy, atomic force microscopy, transmission electron microscopy, X-ray diffraction and dynamic light scattering, respectively; '+' and '–' indicates positive and negative, respectively ; ± represents standard deviation

Table S4: Time (0-24 h) dependent analysis of nanoparticle size and dissolution of metal ions in sterile nutrient broth (1X).

Time (h)	Concentration of NPs	Size of NPs (nm) by DLS in nutrient broth		Metal ion release (µg ml^{-1})		Metal ion release (%)	
		Ag-NPs	ZnO-NPs	Ag^{+}	Zn^{2+}	Ag^{+}	Zn^{2+}
t_0 (0)	1000 µg ml^{-1}	244±9	323±10.5	10±2	10.6±3.7	1.03	1.06
t_1 (3)	1000 µg ml^{-1}	267.3±12.2	345±5	18±3	14±2	1.8	1.43
t_2 (6)	1000 µg ml^{-1}	286.6±6.6	339.3±8.5	20±7	19.3±4.7	2.03	1.93
t_3 (12)	1000 µg ml^{-1}	278.6±3.7	337.6±15.2	31±10	20±5.8	3.13	2.06
t_4 (24)	1000 µg ml^{-1}	297.3±12	352±4	39±8.5	26.3±5	3.93	2.63

Table S5: Bacterial cultures used in the present study

S. No.	Accession Number	Taxonomic designation	Source	Plant growth promoting traits
1.	ATCC 9043, 2351 (T)	*Azotobacter chroococcum* Beijerinck 1901 (Type strain)	Soil	N_2 fixation, L-carnitine production
2.	2095	*Bacillus thuringiensis*	Soybean rhizosphere	Zinc solubilization
3.	2126	*Pseudomonas mosselii*	Soybean rhizosphere	Zinc solubilization, siderophore production
4.	NAIMCC-B-00863	*Sinorhizobium meliloti*	Not mentioned	Symbiotic N_2 fixer (*Medicago sativa*)

Table S6: Scheme of bacterial growth under the influence of varying concentrations of NPs

NPs Used	Treatment (µg ml^{-1}) (i)				Treatment (ii)				Treatment (µg ml^{-1}) (iii)
	A	B	P	S	A	B	P	S	
Ag-NPs	125	125	125	125	-	-	-	-	125
	250	250	250	250	-	-	-	-	250
	500	500	500	500	-	-	-	-	500
	1000	1000	1000	1000	-	-	-	-	1000
ZnO-NPs	125	125	125	125	-	-	-	-	125
	250	250	250	250	-	-	-	-	250
	500	500	500	500	-	-	-	-	500
	1000	1000	1000	1000	-	-	-	-	1000

A= *A. chroococcum*; B= *B. thuringiensis*; P= *P. mosselii*; S= *S. meliloti*. Each individual experiment was replicated three times

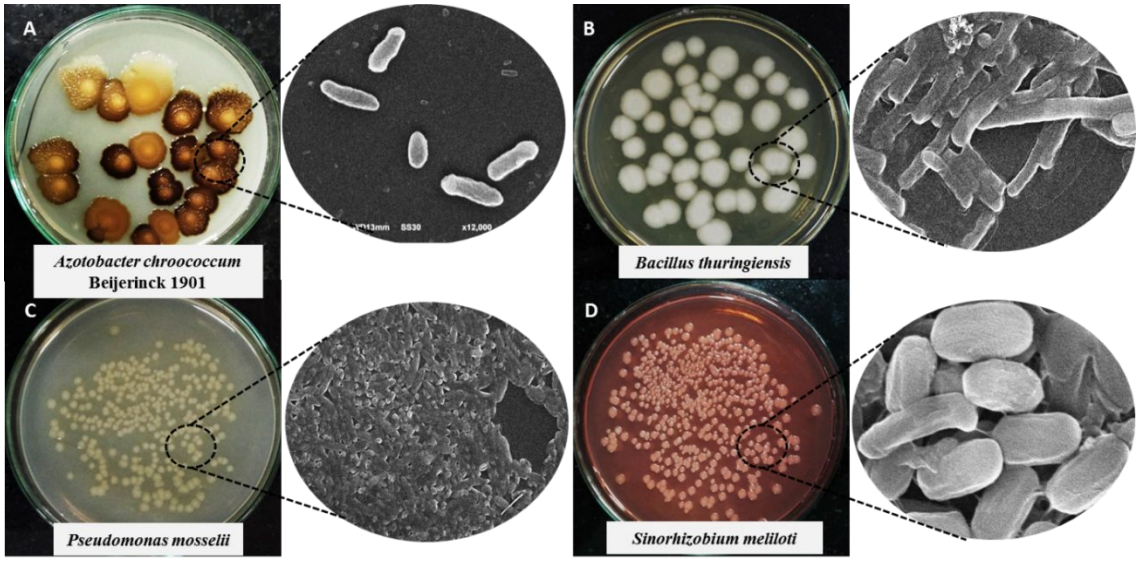

Figure S1. Colonial characteristics of beneficial soil bacteria used in this study. A: *A. chroococcum*; B: *B. thuringiensis*; C: *P. mosselii*; and D: *S. meliloti*.

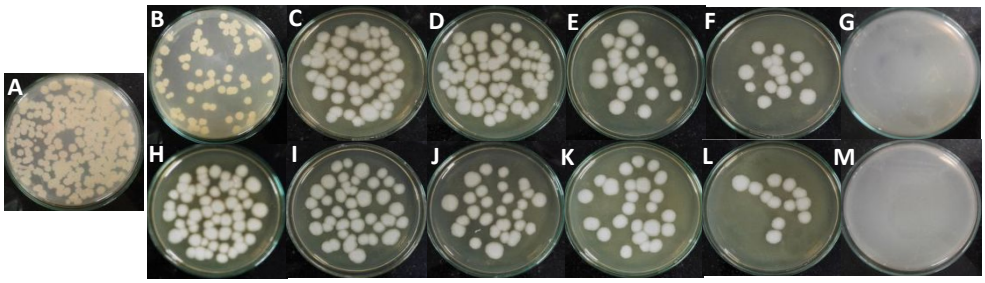

Figure S2. Concentration dependent inhibition of cell viability of *B. thuringiensis* by NPs: control (A), 62.5 (B), 125 (C), 250 (D), 500 (E), 1000 (F), 1500 (G) µgAgNPs ml^{-1}; 62.5 (H), 125 (I), 250 (J), 500 (K), 1000 (L) and 1500 (M) µgZnONPs ml^{-1}.

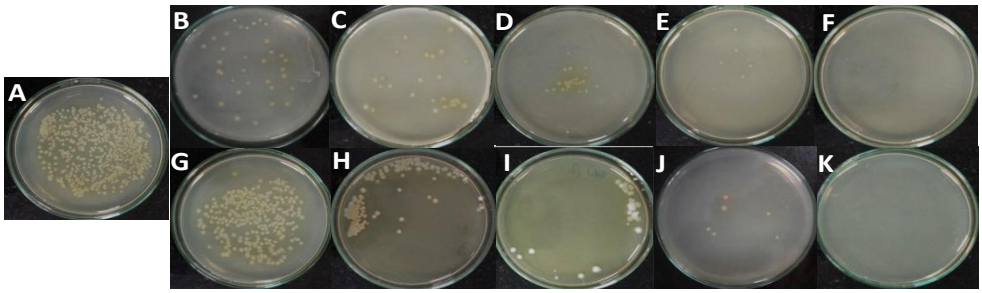

Figure S3. Concentration dependent inhibition of cell viability of *P. mosselii* by NPs: control (A), 62.5 (B), 125 (C), 250 (D), 500 (E) and 1000 (F) µgAgNPs ml^{-1}; 62.5 (G), 125 (H), 250 (I), 500 (J) and 1000 (K) µgZnONPs ml^{-1}.

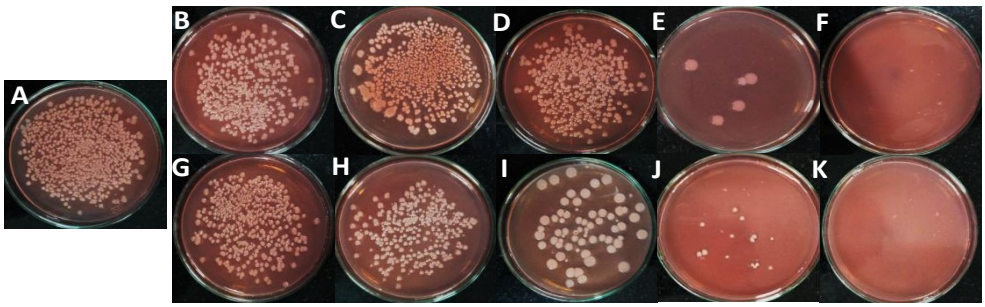

Figure S4. Concentration dependent inhibition of cell viability of *S. meliloti* by NPs: control (A), 62.5 (B), 125 (C), 250 (D), 500 (E) and 1000 (F) µgAgNPs ml^{-1}; 62.5 (G), 125 (H), 250 (I), 500 (J) and 1000 (K) µgZnONPs ml^{-1}.

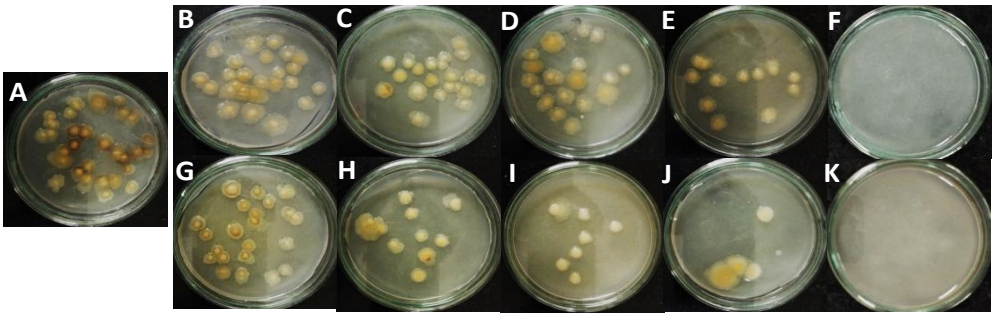

Figure S5. Concentration dependent inhibition of cell viability of *A. chroococcum* by NPs: control (A), 62.5 (B), 125 (C), 250 (D), 500 (E) and 1000 (F) µgAgNPs ml^{-1}; 62.5 (G), 125 (H), 250 (I), 500 (J) and 1000 (K) µgZnONPs ml^{-1}.

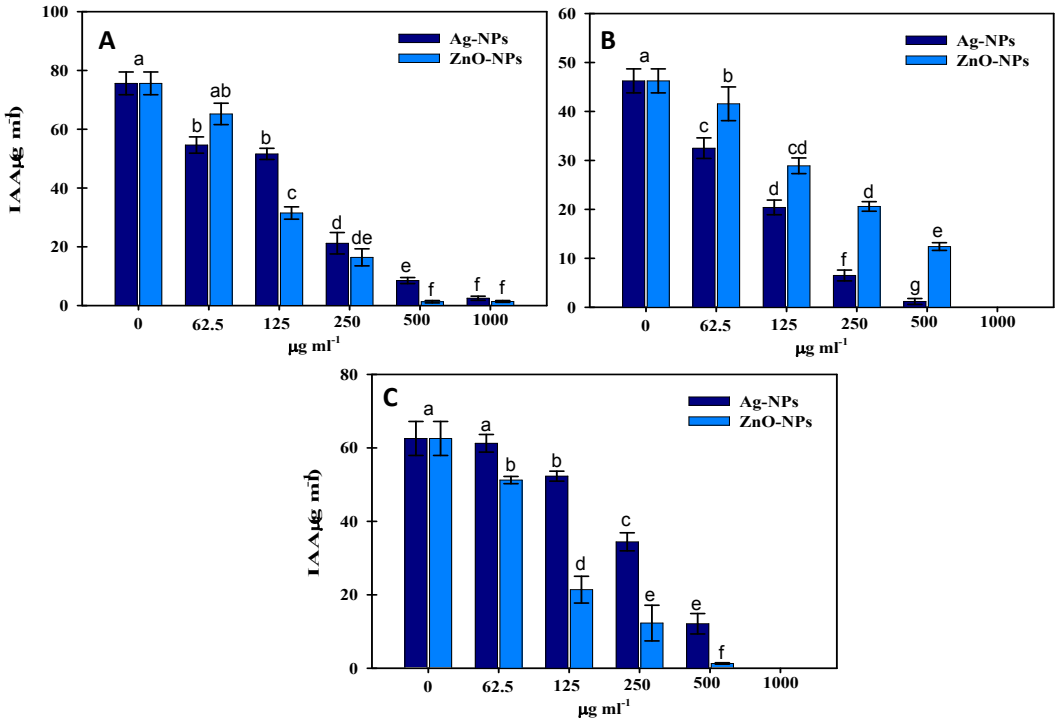

Figure S6. Bioassay of indole acetic acid (IAA) secretion by *P. mosselii* (A), *S. meliloti* (B) and *A. chroococcum* (C) grown in LB broth treated with 62.5-1000 µg ml^{-1} each of Ag-NPs and ZnO-NPs. Different letters on bars denotes significant difference (P≤0.05) according to DMRT.

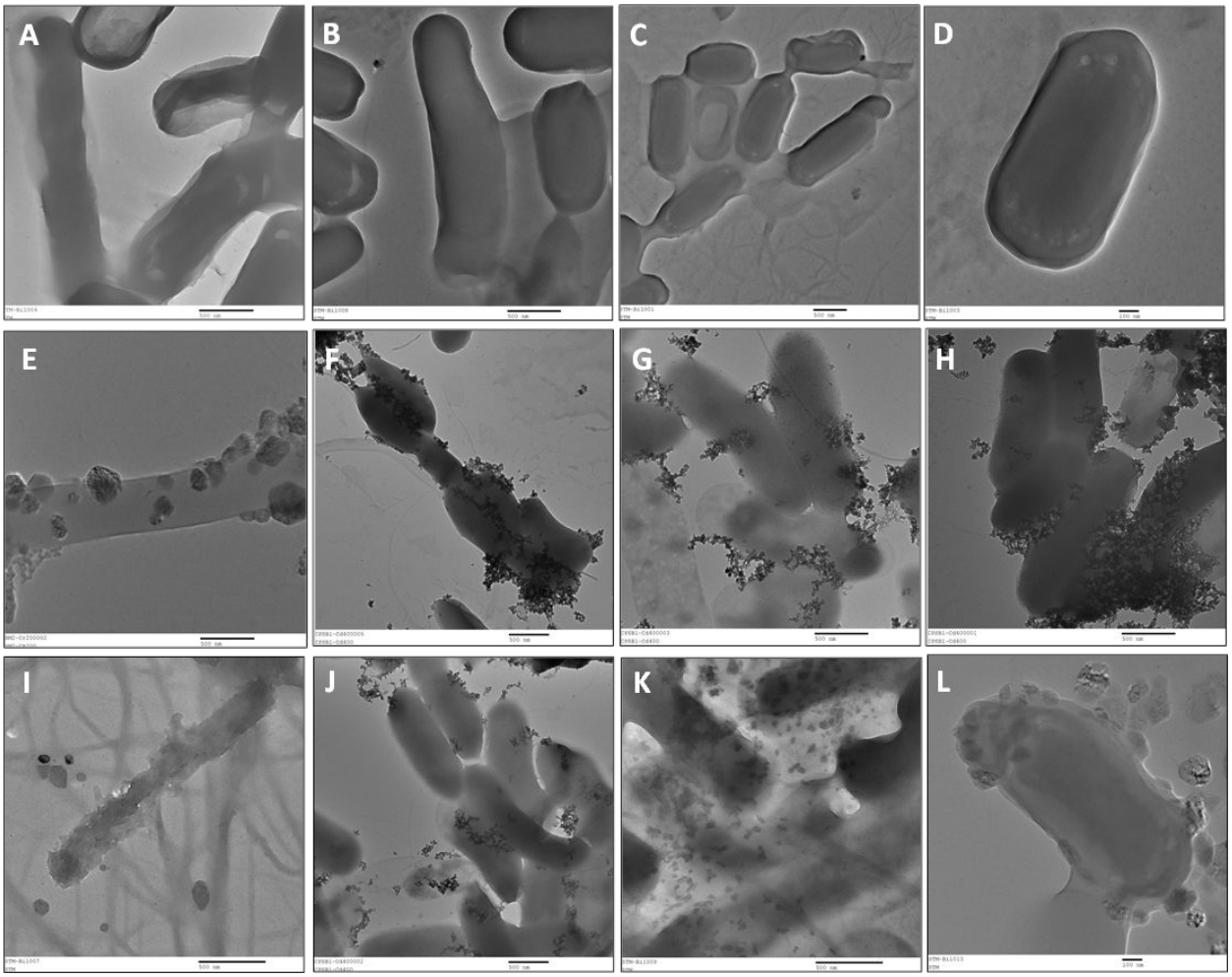

Figure S7. Transmission electron micrographs of bacterial strains; control cells of *B. thuringiensis* (A), *P. mosselii* (B), *S. meliloti* (C) and *A. chroococcum* (D), *B. thuringiensis*+1000 µgAg-NPs ml^{-1} (E), *P. mosselii*+500 µgAg-NPs ml^{-1} (F), *S. meliloti*+250 µgAg-NPs ml^{-1} (G), *A. chroococcum*+500 µgAg-NPs ml^{-1} (H), *B. thuringiensis*+1000 µgZnO-NPs ml^{-1} (I), *P. mosselii*+500 µgZnO-NPs ml^{-1} (J), *S. meliloti*+250 µgZnO-NPs ml^{-1} (K) and *A. chroococcum*+500 µgZnO-NPs ml^{-1} (L).

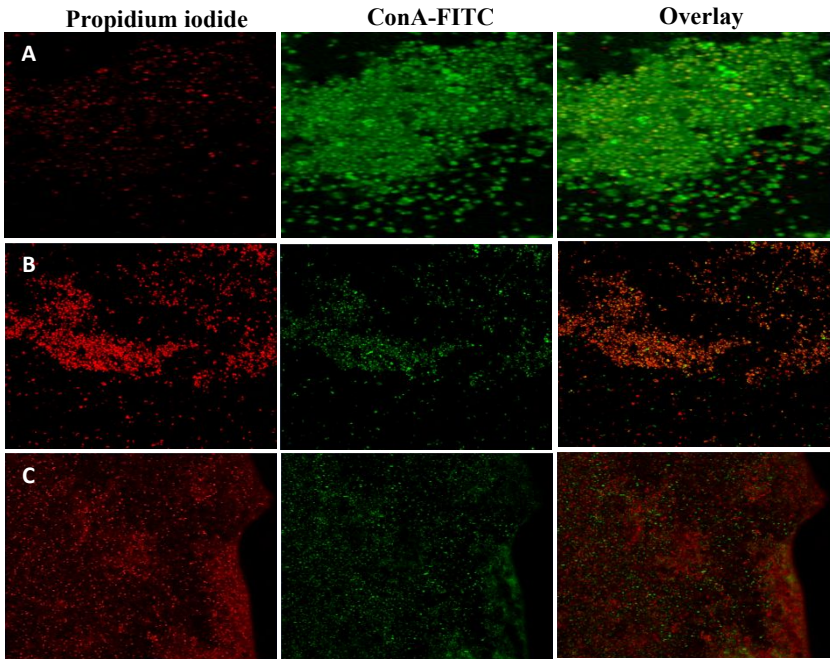

Figure S8. CLSM images (at 400X) of *B. thuringiensis* biofilm. Panel A represents untreated biofilm of *B. thuringiensis*. Red fluorescence depicts propidium iodide stained bacterial cells while green fluorescence of ConA-FITC indicates the presence of EPS. Panels B and C represent CLSM images of *B. thuringiensis* biofilm observed at 1000 µg ml^{-1} each of Ag-NPs (B) and ZnO-NPs (C).

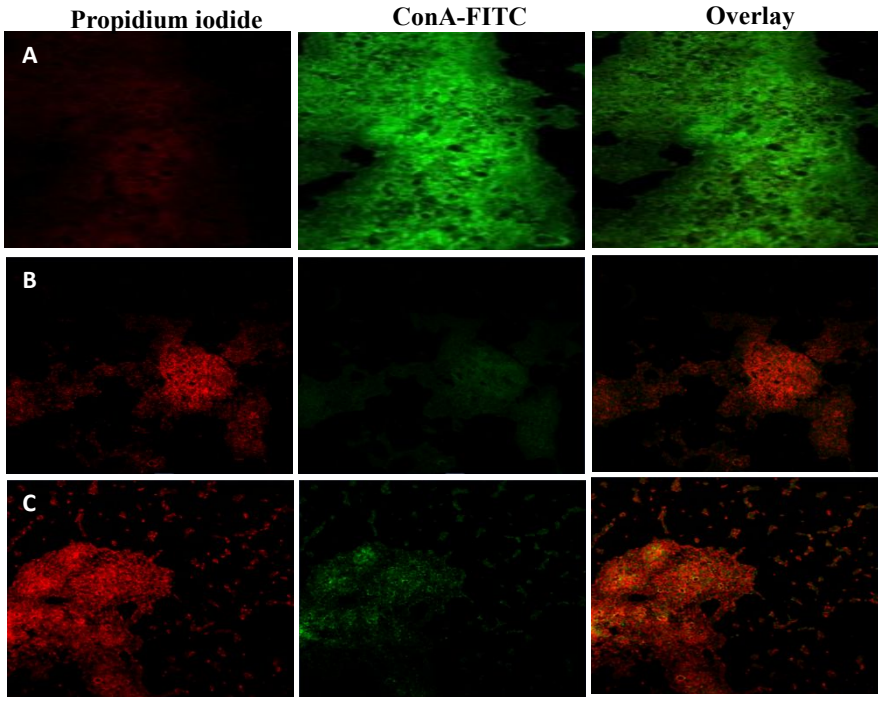

Figure S9. CLSM images (at 400X) of *P. mosselii* biofilm. Panel A represents untreated biofilm of *P. mosselii*. Red fluorescence depicts propidium iodide stained bacterial cells while green fluorescence of ConA-FITC indicates the presence of EPS. Panels B and C represent CLSM images of *B. thuringiensis* biofilm observed at 500 µg ml^{-1} each of Ag-NPs (B) and ZnO-NPs (C).

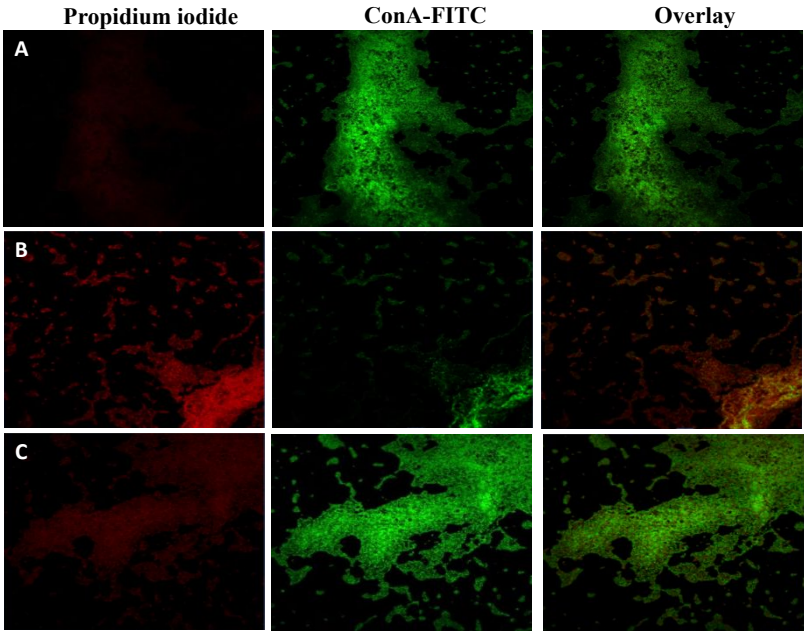

Figure S10. CLSM images (at 400X) of *S. meliloti* biofilm. Panel A represents untreated biofilm of *S. meliloti*. Red fluorescence depicts propidium iodide stained bacterial cells while green fluorescence of ConA-FITC indicates the presence of EPS. Panels B and C represent CLSM images of *B. thuringiensis* biofilm observed at 500 µg ml^{-1} each of Ag-NPs (B) and ZnO-NPs (C).

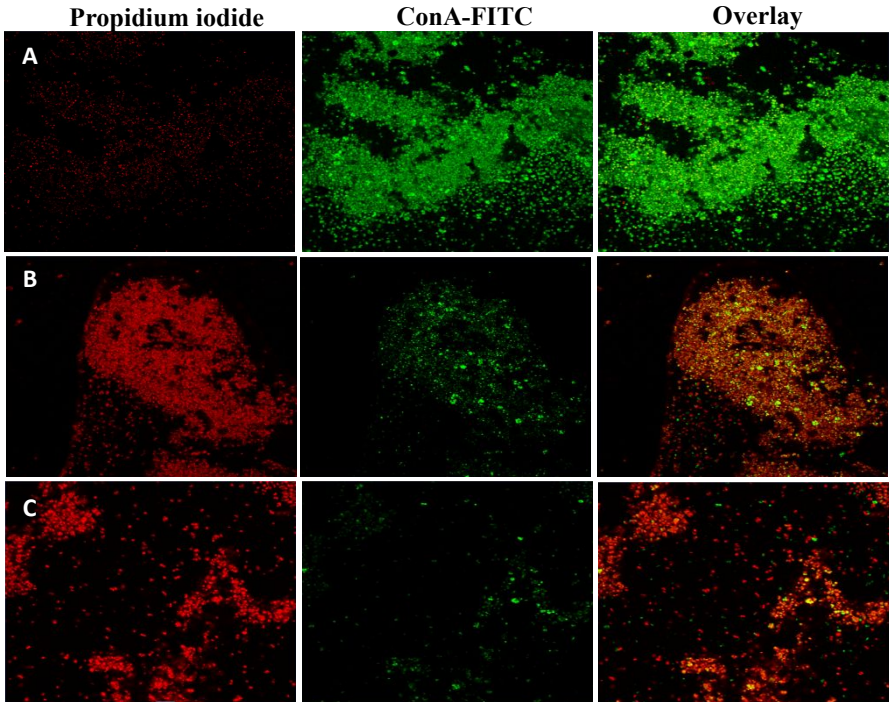

Figure S11. CLSM images (at 400X) of *A. chroococcum* biofilm. Panel A represents untreated biofilm of *A. chroococcum*. Red fluorescence depicts propidium iodide stained bacterial cells while green fluorescence of ConA-FITC indicates the presence of EPS. Panels B and C represent CLSM images of *B. thuringiensis* biofilm observed at 500 µg ml^{-1} each of Ag-NPs (B) and ZnO-NPs (C).

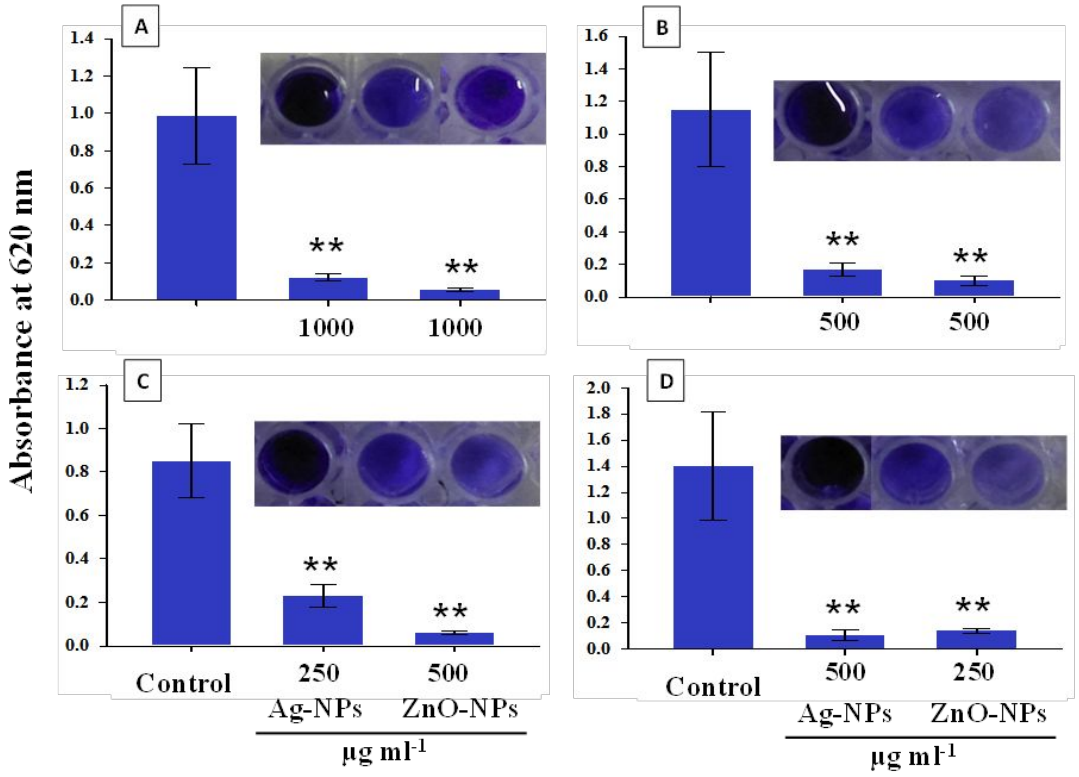

Figure S12. Bar diagrams (A-D) represents the absorbance of crystal violet retained by cells of *B. thuringiensis* (A), *P. mosselii* (B), *S. meliloti* (C) and *A. chroococcum* (D) after NPs exposure. Asterisks indicate significant difference at **P < 0.001.

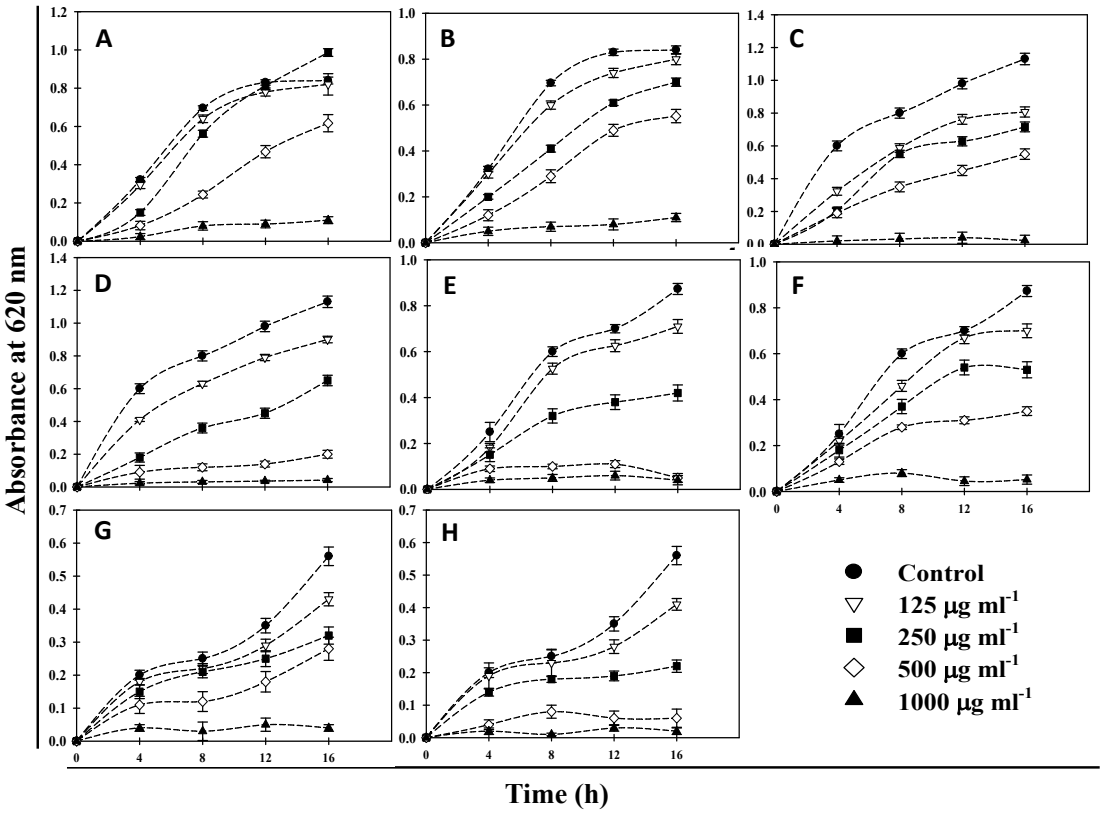

Figure S13. Time (0-16 h) and concentration (125–100 µg ml^{-1}) dependent growth inhibition of bacterial strains. A: *B. thuringiensis*+Ag-NPs, B: *B. thuringiensis*+ZnO-NPs, C: *P.*

mosselii+Ag-NPs, D: *P. mosselii*+ZnO-NPs, E: *S. meliloti*+Ag-NPs, F: *S. meliloti*+ZnO-NPs, G: *A. chroococcum*+Ag-NPs and H: *A. chroococcum*+ZnO-NPs.

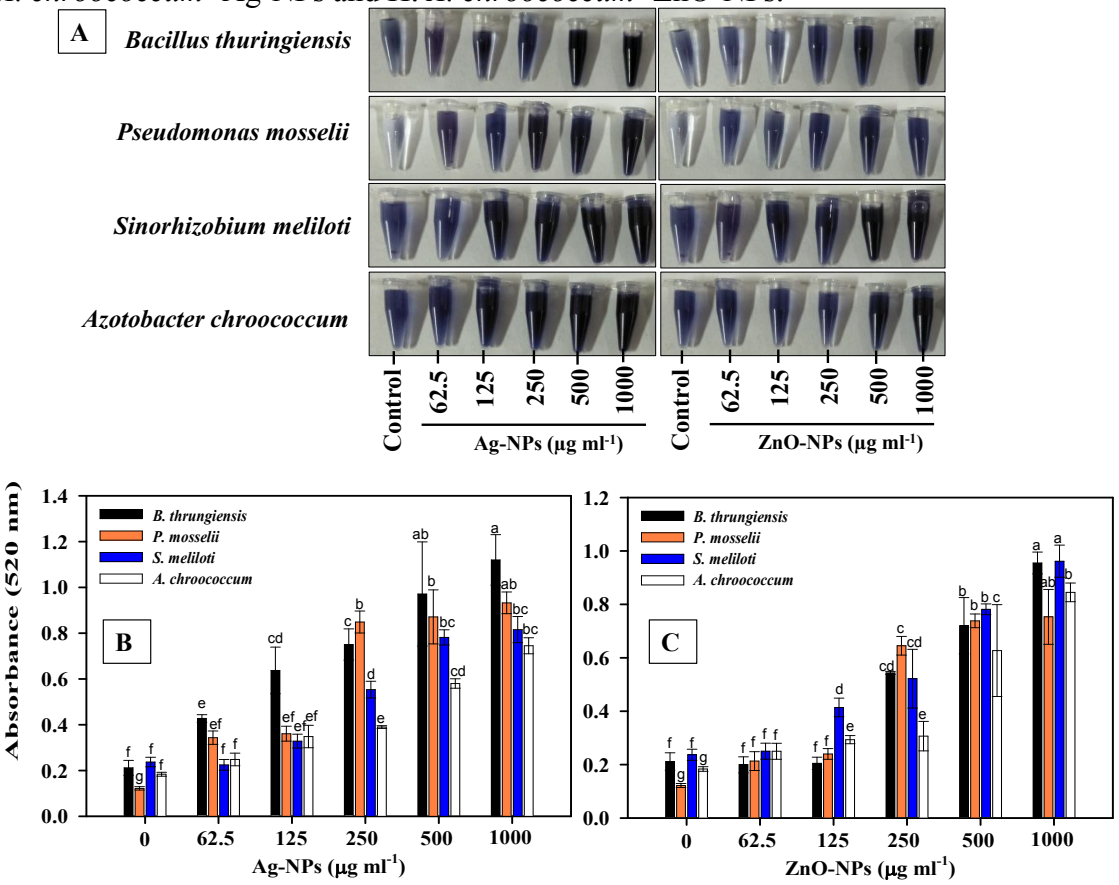

Figure S14. NBT staining of bacterial cells under NPs stress: Intracellular development of blue color formazan by *B. thuringiensis, P. mosselii, S. meliloti* and *A. chroococcum* under varying concentrations (62.5-1000 µg ml^{-1}) of Ag-NPs and ZnO-NPs. Panel A represents generation of superoxide radicals while Panels B and C show spectrophotometric quantification of superoxide radicals generated by Ag-NPs (B) and ZnO-NPs (C). Different letters on bars denotes significant difference at P≤0.05 according to DMRT.